Ocean and Coastal Management 219 (2022) 106060

Contents lists available at ScienceDirect

Ocean and Coastal Management

journal homepage: www.elsevier.com/locate/ocecoaman

The response of salt intrusion to changes in river discharge, tidal range, and winds, based on wavelet analysis in the Modaomen estuary, China

Wenping Gong [a,b,d], Zhongyuan Lin [c,e,*], Heng Zhang [a,b,d], Hongyang Lin [a,f]

[a] Southern Marine Science and Engineering Guangdong Laboratory (Zhuhai), Zhuhai, 519000, China
[b] School of Marine Science, Sun Yat-sen University, Guangzhou, 510275, China
[c] Key Laboratory of Pearl River Estuary Regulation and Protection of Ministry of Water Resources, Guangzhou, 510611, China
[d] Pearl River Estuary Marine Ecosystem Research Station, Ministry of Education, Zhuhai, 519082, China
[e] Pearl River Water Resources Research Institute, Guangzhou, 510611, China
[f] State Key Laboratory of Marine Environmental Science, College of Ocean and Earth Sciences, Xiamen University, Xiamen, 361102, China

ARTICLE INFO

Keywords:
Salt intrusion
Cross-shore wind
Alongshore wind
Cross wavelet
Wavelet coherence

ABSTRACT

Salt intrusion is a serious environmental problem and is affected by many external forcings, and Modaomen Estuary in China's Pearl River Delta is no exception. Based on the cross-wavelet and wavelet coherence analysis, this study investigated the responses of salt intrusion to different forcings, including tidal range, river discharge, alongshore and cross-shore winds, in different timescales. In the intraseasonal timescale, the response times for the salt intrusion to the tidal range, river discharge, alongshore and cross-shore winds are 1.8–6.2, 1.2–9.2, 3.6–10.5, and 3.0–10.4 days, respectively. When averaging the magnitude of response in each winter over 2004–2016, it is found that the most important forcing in influencing the interannual variability of salt intrusion is the tidal range, followed by cross-shore wind, alongshore wind, and river discharge. The winds have great impacts on the salt intrusion, in which a strong downwelling-favorable alongshore wind enhances the salt intrusion and in general, a down-estuary cross-shore wind imposes a similar effect, although its effect varies considerably. This study is of implications for the regional water resource management in the Modaomen Estuary.

1. Introduction

Salt intrusion is a serious environmental problem for many estuaries and is expected to become more serious owing to elevated sea level, reduced river discharge, and deepened estuarine bathymetry by both climate change and human interventions. Salt intrusion is affected by many external forcings, including river discharge, tides, winds, and waves (MacCready and Geyer, 2010), among which the effects of river discharge and tides are mostly studied. The wind effect on salt intrusion has received more attention in recent decades (e.g., Fong and Geyer, 2001; Banas et al., 2004; North et al., 2004; Scully et al., 2005; Li and Li, 2011 and 2012). The effect of wind can be separated into two components: one is by the local wind and another one is by the remote wind. The distinction of local and remote winds is usually arbitrary, here we refer to the local wind as that working inside the estuary, while the remote wind is that working outside the estuary. The local wind directly acts on the water surface of the estuary and changes the mixing and circulation in the estuary, which consequently alters the salt intrusion. The remote wind modulates the water elevation and salinity at the estuary mouth and impacts the salt intrusion in an indirect way.

As the external forcings are generally unsteady, the salt intrusion is mostly in a transient state adapting to the changing forcings. The response can be expressed by a function with a certain magnitude and a time lag (Kranenburg, 1986; MacCready, 1999 and 2007; Lerczak et al., 2009). The time lag is dependent on the contrast between the intrinsic timescale of the estuary and the timescale of the changing external forcing. When the intrinsic timescale is much shorter than the external one, the salt intrusion keeps pace with the change in external forcing and is in a state of equilibrium. In another extreme, when the intrinsic timescale is quite longer than the external one, the adjustment of the salt intrusion can not keep pace with the change of the external forcing, and the salt intrusion can hardly reach an equilibrium. Amid these two extrema, the salt intrusion lags behind the change in the external forcing with a certain time lag. The intrinsic timescale is determined by the

* Corresponding author. Pearl River Water Resources Research Institute, Guangzhou, 510611, China.
E-mail address: lzy900414@126.com (Z. Lin).

https://doi.org/10.1016/j.ocecoaman.2022.106060
Received 1 March 2021; Received in revised form 22 December 2021; Accepted 20 January 2022
Available online 5 February 2022

background state of the estuary and the mean condition of the external forcings (Lerczak et al., 2009). Asymmetry in the adjustment timescale is noted between the strengthening and weakening stages of the external forcing in an estuary, and is attributed to the nonlinearity of salt intrusion in adapting to the external forcing (Chen, 2015).

Due to the unsteadiness of external forcings and salt intrusion, the wavelet analysis has proved to be a robust way to identify the response magnitude and time lag between different variables (Torrence and Compo, 1998; Grinsted et al., 2004). It has been widely used in nonstationary data analysis in oceanography and estuarine research (Liu et al., 2014; Yuan et al., 2017; Forbes and Xie, 2018).

Modaomen Estuary (Fig. 1) is one of the major estuaries in the Pearl River Delta (PRD), which is located in southern China and adjacent to the South China Sea, whose hydrodynamics exhibits distinct seasonal variations. The wet summer season (from May to September) coincides with a prevalent mild Southwesterly wind and the dry winter season (December to February) is coincident with a strong Northeasterly wind. It is micro-tidal, and partially mixed or highly stratified during the winter dry season, the period of concern in this study. It carries most of the freshwater from the Pearl River into the South China Sea and has several water treatment plants along its course, which are fundamental for freshwater supply in the surrounding areas, including Macau, Zhuhai, and Zhongshan cities. The water withdrawal at the plants suffers from contamination by elevated salinity and their functions are interrupted for several days or weeks during the dry winter season. A thorough understanding of the salt intrusion dynamics is thus essential to the operation of these plants.

The salt intrusion in the Modaomen Estuary has been extensively studied, which is mostly concentrated on the effects of river discharge and tidal mixing (Gong and Shen, 2011; Liu et al., 2014). The wind effect is less studied and remains to be explored. In this study, we analyze the response of salt intrusion in the estuary to the changing river discharge, tidal range, and winds through wavelet analysis. As mentioned above, the response to a specific external forcing depends on the background state of the estuary and the mean conditions of several external forcings, and thus the effects of different forcings can be interactive. The aims of this study are thus to 1) identify the dominant time scales of the correlation between the salt intrusion and different external forcings, including river discharge, tides, and winds. Here the winds comprise alongshore (remote) and cross-shore (local) ones. 2) examine the response functions of the salt intrusion to different forcings, including the magnitude and time lag; 3) discuss the dependence of the correlation between the salt intrusion and a single forcing variable on variations of other external forcings.

As the wind forcing in modulating the salt intrusion in Modaomen Estuary has not been well investigated before, this study can be considered as a first step to identify the winds' effect, and the preliminary results of this wavelet analysis can be a useful effort for further dynamical study in the future.

2. Data and methodology

In this study, we collected time series data of daily maximum surface salinity at several stations along the estuary, daily river discharge at the upstream (Gaoyao Station, GY, see Fig. 1) of the West River, which is the main branch of the Pearl River, daily maximum tidal range at the Shibi Station, Hongkong (HK, see Fig. 1) and wind data in the PRD. The daily maximum salinity at the seven stations in the lower and middle estuary from 2004 to 2016 was obtained from the Zhongshan Water Resource Management Bureau (http://water.zs.gov.cn/xxml/fzjzxx/xqbg/), and the seven stations are Dachongkou (DCK), Denglongshan (DLS), Lianshiwan (LSW), Majiao (MJ), Nanzhen (NZ), Xihe (XH), and Quanlu (QL) stations from downstream to upstream, respectively. The period in each winter is from 1st, December to next 28th, February, with a gap in 2010–2011, when the period was from 1st, December to next 29th, January. The wind data is the hourly data from NCEP (National Centers for Environmental Prediction) with a spatial resolution of 0.205° × 0.204°. The wind was spatially averaged within a chosen region that covers the Modaomen Estuary and part of the outside continental shelf (see Lin et al., 2019). The justification for choosing such an area was explained in detail in Lin et al. (2019) and is not repeated here.

To do the subsequent analysis, all data were converted into daily data. The salinity data at the seven stations were subject to EOF (Empirical Orthogonal Function) analysis, and the first mode was shown to represent more than 70% of the variance. The temporal variation of the first mode (PC1) is representative of the change of the surface

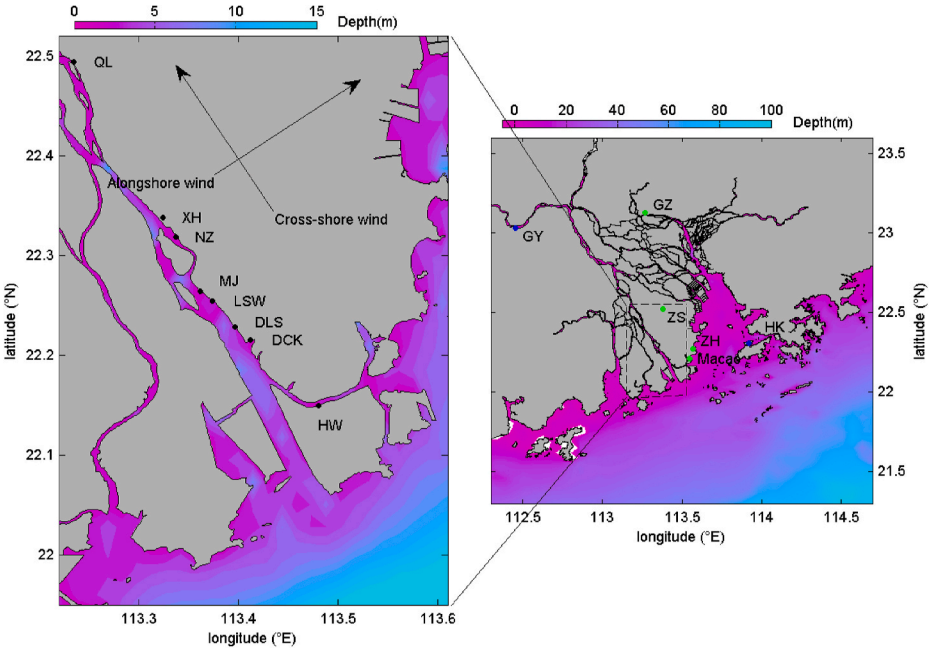

Fig. 1. Map of the Modaomen Estuary area and location of the stations. The arrows schematically show the alongshore and cross-shore wind directions. The wind inclination angle, which is the angle between the wind direction and the coastline orientation (25° from the north). Station numbers are given sequentially from downstream to upstream.

salinity, and thus the salt intrusion in the estuary. The wind was decomposed into two components: alongshore and cross-shore. The alongshore is defined as the direction of shoreline extension in the PRD, which is 22.5° rotating eastward from the north. The cross-shore direction is that orthogonal to the alongshore direction. For the alongshore wind, positive means the Southwesterly wind, and for the cross-shore wind, positive means the Southeasterly wind.

Wavelet is a method to convert the data from time-space into frequency space and determines both the dominant modes of variability and their variation with time. Different from the Fourier analysis, it can resolve the variation of spectral energies with time as it accentuates the importance of the nearby data for a specifically chosen time. The main advantage of wavelet analysis is that it does not require a presumed distribution of data and can examine the phase characteristics and correlations between two non-stationary time series data in terms of time-frequency analysis (Lonnie and Huang, 1996). The wavelet analysis is able to find localized periodicities (or bands) that can be linked to specific processes. In this study, the continuous wavelet transform (CWT) method was used to identify the multi-scale characteristics of salinity, tidal range, river discharge, and wind data, and the cross wavelet and wavelet coherence analysis was employed to examine the nonlinear correlations among these variables.

The Morlet wavelet was used in this study to calculate the continuous wavelet transform because it oscillates with a mean value of zero and is particularly suitable for nonstationary signals. It shows desired symmetry and consists of a plane wave modulated by a Gaussian distribution (Farge, 1992):

$$\psi(t) = \exp\left(-\frac{t^2}{2}\right) exp(j\Omega_0 t) \tag{1}$$

where j is the imaginary unit, and Ω_0 is the central frequency.

For a given wavelet signal $x(t)$, the wavelet transform can be defined as

$$WT_x(a,b) = \frac{1}{\sqrt{a}} \int x(t)\psi^*\left(\frac{t-b}{a}\right) dt \tag{2}$$

where a is a scale factor that can make a basic wavelet $\psi(\Omega)$ flexible;b is a time-shifting factor and reflects movement in time; and $\mathrm{WT}_x(a,b)$ is the wavelet transform coefficient which reflects the variations in time series on a certain time scale.

For the Morlet wavelet, the corresponding relationship between the scale factor of the time series and the period T can be described as:

$$T = \frac{4\pi}{\Omega_0 + \sqrt{2+\Omega_0^2}} \times a \tag{3}$$

The cross wavelet transforms (*XWT*), combining the wavelet transform and cross-spectrum analysis, is a signal analysis technique of multi-scale wavelet transform. *XWT* can be used in multiple time-frequency analyses of two-time series (Grinsted et al., 2004). It can also determine the correlations by describing the phase relationship in the time-frequency space for two-time series and can accurately diagnose the time lag and phase structures between them.

Given two-time series X and Y with wavelet transforms $W_n^X(s)$ and $W_n^Y(s)$, the cross-wavelet spectrum can be defined as follows (Torrence and Compo, 1998):

$$W_n^{XY}(s) = W_n^X(s) W_n^{Y^*}(s) \tag{4}$$

where $W_n^{Y^*}(s)$ is the complex conjugate of $W_n^Y(s)$. s is the time series, and n is the length of s. The cross-wavelet common power can be defined as $\left|W_n^{XY}(s)\right|$: the greater this value, the higher the mutual correlation.

The component of $W_n^{XY}(s)$ is used to describe the phase between the two-time series, and the circular mean of the phase over regions with >5% statistical significance is used to quantify the phase relationship. The circular mean of a set of angles α_i (i=1,2, …,n) is defined as follows:

$$\overline{\alpha} = \arg(\overline{x}, \overline{y}), \overline{x} = \sum_{i=1}^{n} \cos(\alpha_i), \overline{y} = \sum_{i=1}^{n} \sin(\alpha_i) \tag{5}$$

Cross wavelet phase angles are represented by arrows in the wavelet figures. The arrow pointing right denotes in phase, pointing left means anti-phase, pointing down indicates a lag of 90°, and pointing up shows a lead of 90°.

Though the cross-wavelet has the strength to detect the relationship between two-time series, it can only reveal regions with high common power, while the coherence wavelet transform can measure the total coherence between two-time series. The wavelet coherence (*WTC*) is the square of the cross-spectrum normalized by the individual power spectra and can be thought of as a localized correlation coefficient in the time-frequency space. It varies from 0 to 1, with high values obtained when wavelets are highly coherent. An important advantage of wavelet coherence is that it indicates coherence even when the common power is low. The wavelet coherence of two-time series is defined as

$$R^2(a) = \frac{\left|\langle s^{-1} W_n^{XY}(s)\rangle\right|}{\left|\langle s^{-1} W_n^{X}(s)\rangle\right| \left|\langle s^{-1} W_n^{Y}(s)\rangle\right|} \tag{6}$$

where <> indicates a smoothing operator in time and frequency.

Generally, the cross-wavelet is used to find regions of high common power and the relative phase of the time series in the time-frequency space, while the wavelet coherence can be utilized to obtain a localized correlation coefficient in time-frequency space between two-time series.

3. Results

3.1. Correlations between the salt intrusion and different external forcings

The time series of PC1 of the daily maximum surface salinity, the daily river discharge, daily maximum tidal range, and daily mean wind stress are shown in Fig. 2. The PC1 exhibits obvious fluctuations in the interannual timescale. The river discharge shows interannual variations as well, keeping fluctuating below 4000 m^3/s before 2015 and jumping to 8000 m^3/s in 2015–2016. The tidal range experiences fluctuations in fortnightly timescale, whereas the monthly mean tidal range keeps almost unchanged. The monthly mean wind stress exhibits larger variability from 2005 to 2011, whereas the variability becomes smaller from 2011 to 2016.

The correlation between the PC1 and a single external forcing shows that an increasing river discharge retards the salt intrusion. Generally, the PC1 is negatively correlated with the river discharge and shows a time lag. Some exceptions occur when the PC1 is positively related to the river discharge, such as in 2006–2007 when a higher river discharge coincided with a larger PC1. A similar relationship holds for the PC1 and the tidal range, with a time lag of about 4 days, same with the results of Lin et al. (2019). Under similar conditions of river discharge and tidal range, the salt intrusion is affected by wind stress. Two notable examples are the variations of the PC1 between January 2007 and February 2007, and between December 2007 and January 2008. The PC1 became smaller in February 2007 (the third blue starred point in 2006–2007, see Fig. 2a) than in January 2007 (the second blue starred point in 2006–2007, see Fig. 2a), when the river discharge and tidal range were similar in these two months (the second and third blue starred points in 2006–2007, see Fig. 2b and c), whereas the wind stress was lower in the former period compared to the latter one (the second and third blue starred points in 2006–2007, see Fig. 2d). The PC1 became larger in January 2008 (the second blue starred point in 2007–2008, see Fig. 2a) than in December 2007 (the first blue starred point in 2007–2008, see Fig. 2a), owing to the increased wind stress (the first and second blue starred points in 2007–2008, see Fig. 2a), even the river discharge was higher in the former period and the tidal range was similar in these two months (the first and second blue starred points in 2007–2008, see

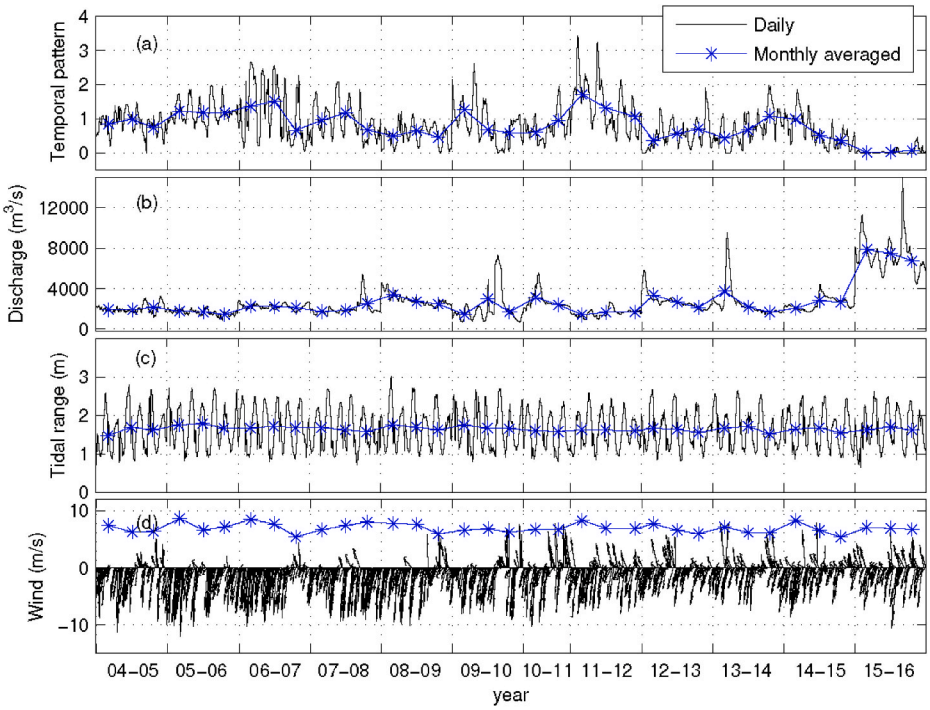

Fig. 2. (a) Time series of the PC1 for the daily surface maximum salinity from 2004 to 2016. (b) Time series of river discharge at Gaoyao Station(GY) during the dry seasons. (c) Time series of daily maximum tidal range. (d) Time series of wind stress from 2004 to 2016. (The blue starred line represents the monthly averaged values.).

Fig. 2b and c). Other examples include those between January 2009 and February 2009 and between December 2011 and January 2012. It indicates that, on the timescale of interannual variation, the river discharge and salt intrusion do not always show a negative correlation, and the winds can impose a greater influence on the salt intrusion, dominating over the effect of river discharge sometimes.

3.2. Response of the salt intrusion to changes in tidal range

The cross-wavelet transform and wavelet coherence analysis of the PC1 and the tidal range, river discharge, cross-shore wind, and alongshore wind are now used to gain more insights into their interactions.

The cross-wavelet result between the PC1 and tidal range is shown in Fig. 3a. It indicates that the PC1 and tidal range have high common power in the narrow band of 12–17 days, indicating there exists a strong correlation between the tidal range and the PC1 in this timescale. The interannual variability of the cross-wavelet in this time band is generally minor. Some exceptions occurred when the river discharge fluctuated greatly, such as in 2009–2010 and 2015–2016, the common power between the PC1 and tidal range became low. This shows that the response of salt intrusion to the tidal range is dependent on the river discharge, as the tidal effect is suppressed when the river discharge increases. The phase shift between the PC1 and tidal range from 2004 to 2016 is 52.9°–131.2°, indicating that the PC1 lags the tidal range by approximately 1.8–6.2 days, consistent with previous results (Gong and Shen, 2011; Lin et al., 2019). This time lag was obtained by multiplying the corresponding period by the phase lag between the two variables.

The wavelet coherence results (Fig. 3b) show a similar pattern that in the timescale of 12–17 days, the PC1 and tidal range have high common power.

From the cross-wavelet results, we averaged the common power and phase shift in each winter, and the results are listed in Table 1. The time lag shows interannual variability, and the common power is positively correlated to the tidal range, with a correlation coefficient of 0.50.

To further identify the response of salt intrusion to increasing or decreasing tidal ranges, we choose the timescale of 12–17 days from January 30th to February 13th in 2012 under the conditions of stable river discharge and smaller common power between the PC1 and winds,

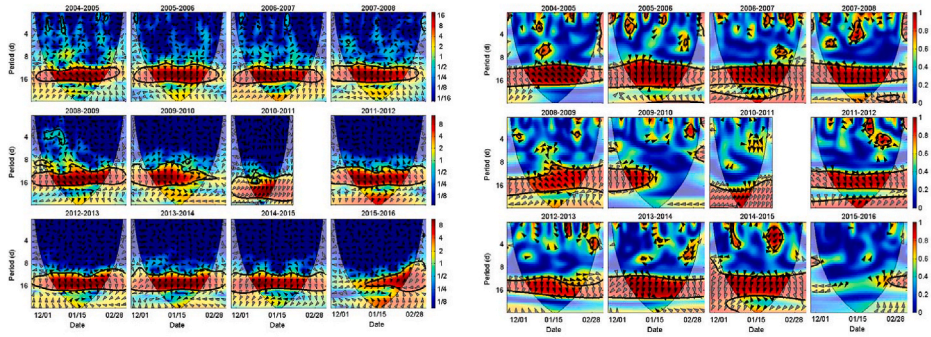

Fig. 3. a) Cross-wavelet and b) wavelet-coherence spectra of the PC1 and tidal range from 2004 to 2016. (The thick black contours enclose regions within which the wavelet power is significant at the 95% confidence level assuming a red-noise null hypothesis. Regions, where the edge effects become important, are shaded with white. Black arrows denote the phase lag between the PC1 and tidal range: → (←) means in-phase (out-of-phase); ↓ (↑) means the PC1 lags (leads) the tidal range changes by 90°).

Table 1
Averaged phase shift, time lag and common power between the PC1 and tidal range, and the averaged tidal range from 2004 to 2016.

Year	phase difference (°)	Lag time (days)	Power	Tide range (m)
04–05	52.9	1.8-2.5	6.28	1.59
05–06	88.3	2.9-4.2	9.85	1.74
06–07	78.2	2.6-3.7	7.70	1.69
07–08	86.5	2.9-4.1	9.38	1.63
08–09	67.7	2.3–3.2	9.10	1.69
09–10	84.4	2.8-4.0	4.93	1.69
10–11	131.2	4.4–6.2	3.83	1.59
11–12	74.1	2.5-3.5	5.66	1.61
12–13	81.2	2.7-3.8	7.99	1.62
13–14	100.4	3.3–4.7	7.34	1.64
14–15	96.5	3.2–4.6	5.28	1.63
15–16	131.5	4.4–6.2	4.15	1.65

as shown in Fig. 4. The phase shift between the PC1 and tidal range (4a) shows an increase-then-decrease transition with the tidal range (4c). The greater phase shift in the increasing stage of the tidal range indicates that when the tidal mixing was enhanced, the salt intrusion became more out-of-phase with the tidal range. The reversed situation occurred during the decreasing stage of the tidal range. These mean that the salt intrusion was quickly shortened with the increasing tidal mixing (more out-of-phase) but slowly lengthened with the decreasing tidal mixing (less out-of-phase), consistent with the results of Chen (2015). In the meantime, the common power between the PC1 and tidal range (4b) was negatively correlated with the river discharge (4d), showing that the tidal effect was suppressed by the elevated river discharge.

3.3. Response of the salt intrusion to changes in river discharge

The results of cross-wavelet and wavelet coherence between the PC1 and river discharge are shown in Fig. 5. During the years with severe salt intrusion (2005–2006, 2006–2007, 2007–2008, 2009–2010, 2011–2012), the common powers between the PC1 and river discharge are high in the time band of 12–17 days. The common power is also high in the time band shorter than 12 days or longer than 17 days in several years, indicating that the variability of river discharge in the timescales shorter than 12 days or longer than 17 days also played some role in the variation of the PC1. The common power becomes nearly zero when the fluctuations of the river discharge are very small in some years (2012–2013, 2015–2016). In general, the common power between the PC1 and river discharge is lower than that between the PC1 and tidal range in the time band of 12–17 days. We attribute it to the fact that the fluctuations of the river discharge are generally smaller and more episodic, such as caused by the opening and closing of the reservoir gates upstream of the Pearl River.

The phase relationship between the PC1 and river discharge shows that there exists strong variability in the response time in seasonal and interannual timescales for the time band of 12–17 days. From Figs. 2b and 5a, when the river discharge less fluctuated, the phase shift was smaller, with a shorter time lag, such as in 2007–2008, 2009–2010, and 2014–2015. It is noted that in 2014–2015, the PC1 kept in phase with the river discharge, suggesting that an enhanced river discharge resulted in an increased salt intrusion, contrary to our general understanding. This abnormality could be induced by change in winds and is explored below.

The wavelet coherence results (Fig. 5b) are not consistent with those of the cross-wavelet ones and show high correlations between the PC1 and the river discharge in the timescales shorter than 12 days or longer than 17 days, as well as the timescale of 12–17 days. It suggests again that the tidal range is more dominant in the timescale of 12–17 days.

The averaged common power, phase difference, and time lag in the timescale of 12–17 days between the PC1 and river discharge in each winter are summarized in Table 2. Overall, the river discharge has no significant correlation with the time lag of the response. This is inconsistent with previous studies in the literature (i.e., Chen, 2015), which concluded that an increased river discharge results in a shortened response time and verse visa. We speculate that many other factors could contribute to this deviation, such as freshwater withdrawal along the

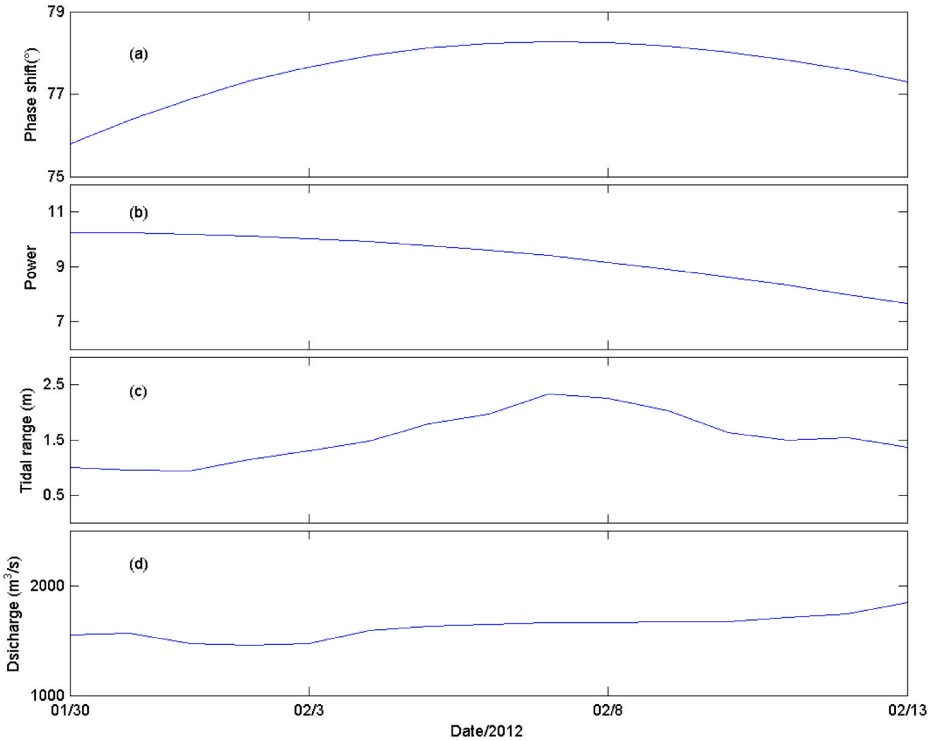

Fig. 4. (a) Time series of the phase shift between the PC1 and tidal range from the cross-wavelet in 2012. (b) Time series of the common power between the PC1 and tidal range from the cross-wavelet in 2012.(c) Time series of daily maximum tidal range in 2012. (d) Time series of river discharge in 2012.

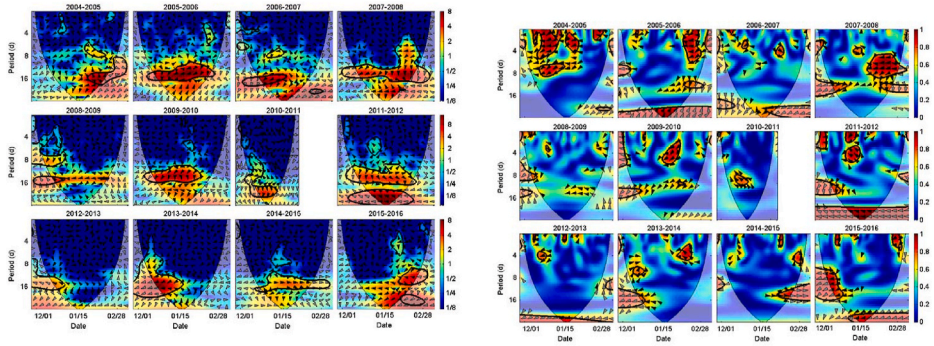

Fig. 5. a) Cross-wavelet and b) wavelet-coherence spectra of the PC1 and river discharge from 2004 to 2016. The formats are similar to Fig. 3.

Table 2
Averaged phase difference, time lag and power between the PC1 and river discharge, and the averaged river discharge from 2004 to 2016.

Year	Phase difference (°)	Time lag (days)	Power	Discharge (m^3/s)
04–05	180.1	6.0–8.5	2.65	1940.7
05–06	131.5	4.4–6.2	5.04	1661.0
06–07	191.3	6.4–9.0	2.63	2202.6
07–08	137.0	4.6–6.5	2.88	1926.3
08–09	185.1	6.2–8.7	2.37	2707.3
09–10	130.1	4.3–6.1	1.94	2790.8
10–11	101.8	3.4–4.8	1.04	2407.1
11–12	100.1	3.3–4.7	2.29	1617.0
12–13	190.7	6.4–9.0	1.02	2612.5
13–14	188.7	6.3–8.9	2.62	2237.0
14–15	35.7	1.2-1.7	1.30	2676.6
15–16	195.8	6.5–9.2	1.82	7320.3

river course, and changes in division ratio between different branches in the Pearl River Network, which resulted in significant changes in river inflow to the Modaomen Estuary, even the river discharge at the upstream (Gaoyao Sta.) did not change much. Moreover, we note that the magnitude of the response is smaller than that between the PC1 and tidal range (Table 2 vs 1).

3.4. Response of the salt intrusion to changes in alongshore wind

The results of cross-wavelet and wavelet coherence between the PC1 and alongshore wind are shown in Fig. 6. The cross-wavelet (Fig. 6a) shows that the PC1 and alongshore wind have high common power in the time band of 12–17 days in several years, though the common power fluctuated through different years. When the river discharge fluctuated dramatically, the common power between the PC1 and alongshore wind was low, so it was with the situation when the wind stress was low. The phase shift between the PC1 and alongshore wind is in the range of 90°–180°, showing a reversed relationship between them. This means that a strong downwelling-favorable wind (Northeasterly wind, negative in the alongshore direction) generates an enhanced salt intrusion. This is expected as a downwelling-favorable wind drives a strong landward transport of higher salinity water from the continental shelf to the estuary. The wavelet coherence analysis (Fig. 6b) shows similar results, and the coherence between the PC1 and alongshore wind is high in 2005–2006, 2007–2008, 2010–2011, and 2013–2014. Similar to the river discharge, the PC1 and alongshore wind have high common power and correlation in timescales shorter than 12 days or longer than 17 days, indicating that the alongshore wind has an effect on the salt intrusion in other timescales than the fortnightly one as the tidal effect.

The overall results are summarized in Table 3, showing that the general time lag is about 180°, indicating the dominant effect of downwelling-favorable winds. The magnitude of response has some

Table 3
Averaged phase difference, time lag and common power between the PC1 and alongshore wind, and the averaged alongshore wind stress from 2004 to 2016.

Year	Phase difference (°)	Time lag (days)	Power	Stress (N/m^2)
04–05	209.5	7.4–10.5	2.24	−0.061
05–06	142.5	5.2–7.4	4.47	−0.080
06–07	164.5	5.8–8.2	1.91	−0.073
07–08	108.6	3.8-5.3	3.95	−0.074
08–09	142.3	4.8-6.8	2.99	−0.071
09–10	173.1	6.1–8.7	2.02	−0.054
10–11	119.6	4.3–6.1	2.21	−0.053
11–12	193.8	6.6–9.4	2.51	−0.075
12–13	202.1	6.8–9.6	2.73	−0.066
13–14	101.1	3.6-5.1	3.74	−0.057
14–15	194.5	6.8–9.6	1.52	−0.066
15–16	183.2	6.2–8.8	1.99	−0.066

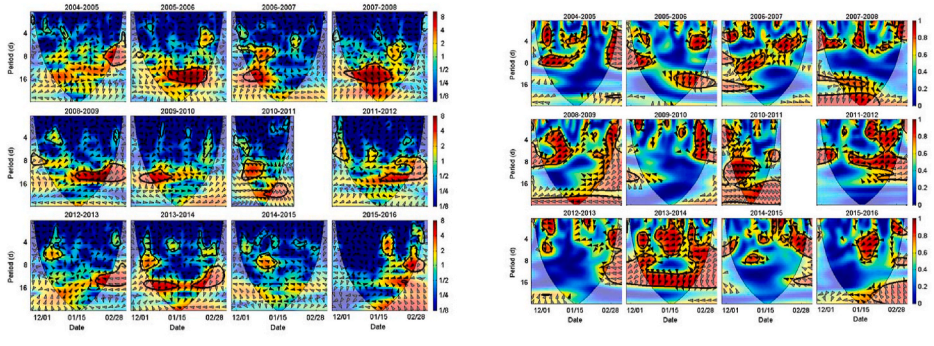

Fig. 6. a) Cross-wavelet and b) wavelet-coherence spectra of the PC1 and alongshore wind from 2004 to 2016. The formats are similar to Fig. 3.

correlation (with a coefficient of −0.43) with the strength of the alongshore wind.

3.5. Response of the salt intrusion to changes in cross-shore wind

The results of cross-wavelet and wavelet coherence analysis are shown in Fig. 7. Similar to that between the PC1 and alongshore wind, the common power (Fig. 7a) in the time band of 12–17 days between the PC1 and the cross-shore wind is high in some years, showing that the cross-shore wind has some close relationship with the salt intrusion. The seasonal variability of the response of salt intrusion to the cross-shore wind is also high.

The phase relationship (Fig. 7a) between the PC1 and cross-shore wind varies greatly, ranging from 0°(in-phase) to 90° and 180°(out of phase), with the out of phase being dominant. The in-phase relationship denotes that an up-estuary/down-estuary wind increases/decreases the salt intrusion, whereas the out-of-phase indicates the opposite situation. The out-of-phase relationship is consistent with Chen and Sanford (2009). The in-phase relationship occurred during both high and low river discharges. It should be noted that the salinity data in this study is at the water surface. When the river discharge is high, a down-estuary wind enhances the surface seaward flow and suppresses the salt intrusion, generating an in-phase relationship between the salt intrusion and cross-shore wind. When the river discharge is low, the estuary is more mixed, and an up-estuary wind can generate a landward (downwind) flow and increase the salt intrusion, again showing an in-phase relationship.

The wavelet coherence (Fig. 7b) shows that the PC1 and the cross-shore wind are correlated at the time band of 12–17 days, and the correlation coefficient varies in different years. The PC1 and cross-shore wind have high common power and correlation in timescales shorter than 12 days or longer than 17 days as well.

The averaged phase difference, time lag, and common power between the PC1 and cross-shore wind in each winter are listed in Table 4. It shows that the phase shift is approximately 180° in most of the time. The common power has a high correlation with the magnitude of the cross-shore wind stress, with a coefficient of −0.61, showing that in general, a stronger down-estuary wind generates a more severe salt intrusion.

4. Discussion

As mentioned above, the response of salt intrusion to a single external forcing is dependent on other forcing variables, here we examine the role of other forcings in affecting the response of salt intrusion to a chosen single forcing. The time series of common power and phase shift between the PC1 and the concerned forcing variable were extracted from the cross-wavelet analysis. The common power is representative of the correlation between the PC1 and the concerned forcing variable.

Table 4
Averaged phase difference, time lag and power between the PC1 and cross-shore wind, and the averaged cross-shore wind stress from 2004 to 2016.

Year	Phase difference (°)	Time lag (days)	Power	Stress (N/m^2)
04–05	220.0	7.3–10.4	3.32	−0.012
05–06	161.1	5.3–7.6	4.62	−0.025
06–07	198.3	6.6–9.3	2.31	−0.024
07–08	89.5	3.0–4.2	5.80	−0.025
08–09	204.4	6.8–9.6	3.59	−0.010
09–10	177.0	5.9-8.3	2.54	−0.005
10–11	116.5	3.9-5.5	2.52	0.003
11–12	156.6	5.2–7.4	1.54	0.004
12–13	196.9	6.5–9.3	2.41	0.013
13–14	164.8	5.4–7.8	3.27	0.012
14–15	211.2	7.0–9.9	3.34	0.006
15–16	194.1	6.5–9.1	2.16	0.014

4.1. Dependence of the response of salt intrusion to tidal range on other variables

The time series of the common power (a and b) and phase shift (c and d) between the PC1 and tidal range are shown in Fig. 8. The corresponding time series of river discharge and wind stresses are also included in the figure for comparison.

Fig. 8a indicates that the common power between the PC1 and tidal range has an obvious negative correlation with the river discharge, and has a time lag to the variation of river discharge. In 2007–2008, 2009–2010, 2012–2013, and 2014–2015, when the river discharge was high, the common power became small, showing that a higher river discharge decreases the correlation between the salt intrusion and tidal range.

Fig. 8b shows the time series of the common power and the wind stress. The wind stress here is the combined one of the alongshore and cross-shore wind stresses, because a single component of wind stress has little impact on the common power and phase shift between the PC1 and tidal range in our results. It displays that the common power is not significantly correlated with the wind stress, suggesting that the wind stress has a relatively low impact on the correlation between the salt intrusion and tidal range. However, in some years when the river discharge was relatively stable, such as 2004–2005, 2005–2006, 2007–2008, 2008–2009, and 2013–2014, the common power was significantly negatively correlated with the wind stress. Low wind stress corresponds to a high correlation between the salt intrusion and tidal range.

The time series of the phase shift between the PC1 and tidal range and that of the river discharge (Fig. 8c) shows that the phase shift has a negative correlation with the river discharge, indicating that higher river discharge induces a shorter response time. Fig. 8d shows the time

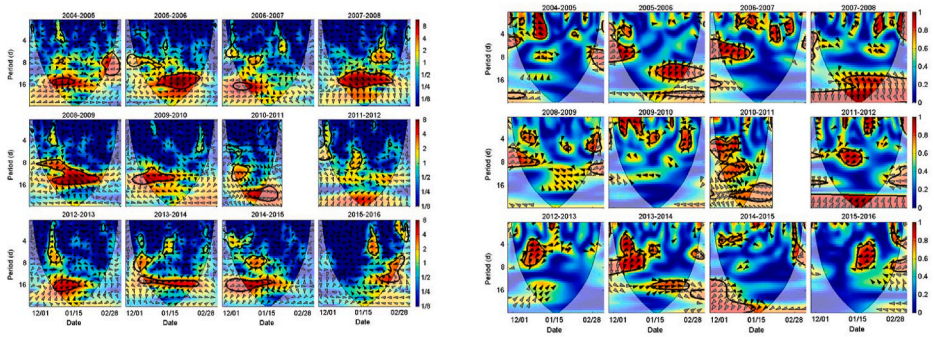

a b

Fig. 7. a) Cross-wavelet and b) wavelet-coherence spectra of the PC1 and cross-shore wind from 2004 to 2016. The formats are similar to Fig. 3.

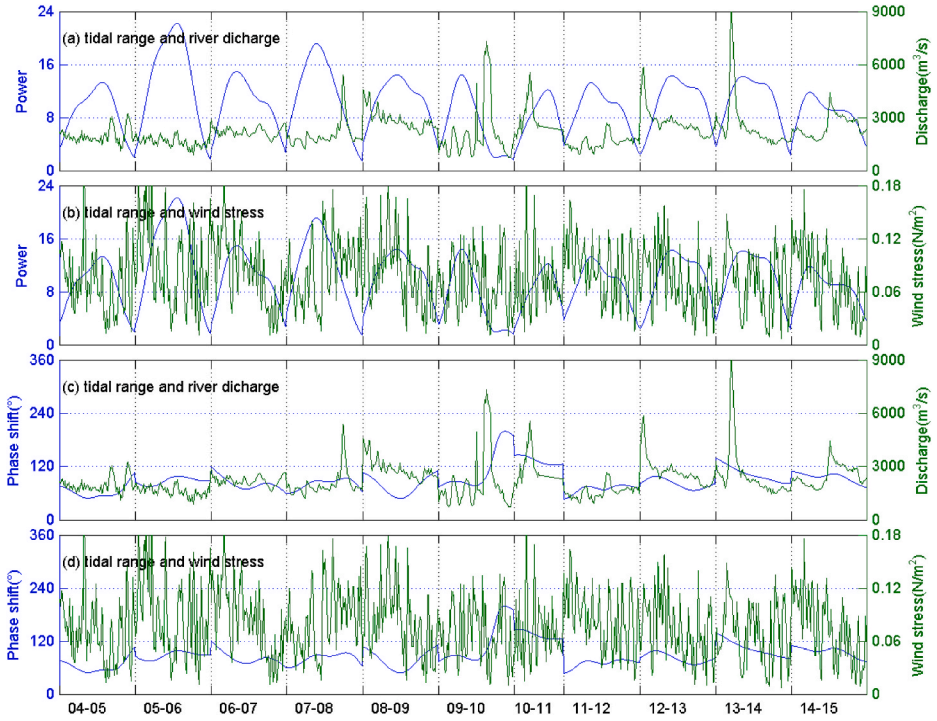

Fig. 8. (a) Time series of the common power between the PC1 and tidal range from the cross-wavelet (blue line) and the river discharge (green line) from 2004 to 2015. (b) Time series of the common power (blue line) and the wind stress (green line). (c) The time series of the phase shift (blue line) between the PC1 and tidal range from the cross-wavelet and the river discharge (green line). (d) Time series of the phase shift (blue line) and the wind stress (green line).

series of the phase shift between the PC1 and tidal range, and the wind stress. The relationship between the phase shift and wind stress was not clear. In the years of stable river discharge, such as 2008–2009, 2011–2012, and 2012–2013, a greater wind stress decreased the response time of the salt intrusion to tidal range, indicated by decreases in phase shift.

Overall, in the intraseasonal timescale, the river discharge poses a distinct impact on the common power and phase shift between the PC1 and tidal range, whereas the wind stress can impact them to some extent in several years.

Fig. 9. (a) Time series of the common power between the PC1 and river discharge from the cross-wavelet (blue line) and the river discharge (green line) from 2004 to 2015. (b) Time series of the common power (blue line) and the wind stress (green line). (c) Time series of the phase shift (blue line) between the PC1 and river discharge from the cross-wavelet and the river discharge (green line). (d) Time series of the phase shift (blue line) and the wind stress (green line).

4.2. Dependence of the response of salt intrusion to river discharge on other variables

The time series of the common power (a and b) and phase shift (c and d) between the PC1 and river discharge are shown in Fig. 9.

Fig. 9a shows the time series of the common power between the PC1 and river discharge and the time series of the river discharge itself. It indicates that the common power has an obvious correlation with the magnitude of river discharge, and an increase in river discharge does increase the correlation. In Fig. 9b, the time series of common power between the PC1 and river discharge and the time series of wind stress is displayed. It indicates that the correlation between them is weak. The time series of phase shifts between the PC1 and river discharge, and the river discharge (Fig. 9c) shows that the phase shift has a weak correlation with the river discharge. The correlation between the phase shift and the wind stress (Fig. 9d) exhibits that when the fluctuation of river discharge is small, an increase in wind stress can shorten the response time of the PC1 to river discharge, such as in 2004–2005, 2007–2008 and 2012–2013. In other years (2005–2006, 2006–2007, 2008–2009, and 2013–2014), and an increase in wind stress can increase the phase shift between the PC1 and river discharge, showing that the effect of wind stress is variable under different conditions.

Overall, in the intraseasonal timescale, the river discharge poses a significant impact on the common power between the PC1 and river discharge, whereas the wind stress and other forcings can impact the phase shift between the PC1 and river discharge.

To further identify the wind effects, we choose a time window for scrutinizing. Time series of the PC1, river discharge, tidal range, cross-shore wind stress, and alongshore wind stress in 2014–2015 are shown in Fig. 10. The gray region represents the significant in-phase correlation between PC1 and river discharge in the wavelet-coherence spectra (Fig. 5). From January 17th to January 31st, the river discharge decreased from a peak value of 4420 m^3/s to 3150 m^3/s, and the PC1 shows a decrease-then-increase transition. The tides ranged from neap to spring and then to neap, and the change in the PC1 had a time lag to the change in tidal range. It is worth noting that the PC1 reached a peak value on January 31st with a greater alongshore wind stress and a moderate tide. A similar situation occurred on February 19th, a greater alongshore wind stress resulted in a larger PC1 under the same magnitude of river discharge, even the tide was a spring one. After February 19th, the changes in PC1 were almost in phase with the river discharge, in which the tides changed from spring to neap, and the up-estuary wind and downwelling-favorable alongshore wind showed a decrease-then-increase transition. Therefore, the in-phase correlation between PC1 and river discharge is caused by the changes in tidal range and winds.

4.3. Dependence of the response of salt intrusion to wind stress on other variables

As the phase shift between the PC1 and alongshore wind stress is highly irregular, we only discuss the dependence of the common power between the PC1 and alongshore wind stress on other forcings. Fig. 11a shows the time series of the common power and the river discharge. It shows that when river discharge was low, the common power was generally high. Fig. 11b shows that the time series of the common power and the alongshore wind stress, and indicates that the common power had no obvious relationship with the magnitude of the alongshore wind stress. As the common power and the phase shift between the PC1 and alongshore wind stress were both variable, the effect of the alongshore wind was more dependent on other forcings or the preexisting state of the estuary. Fig. 11c and d shows that a similar situation occurred for the cross-shore wind, and indicates that when the fluctuation of river discharge was small, the correlation between the cross-shore wind and salt intrusion was relatively high in most years.

Time series of the PC1, river discharge, tidal range, cross-shore wind stress, and alongshore wind stress in 2013–2014 are shown in Fig. 12. The gray region represents the significant in-phase correlation between PC1 and cross-shore wind stress in the wavelet-coherence spectra (Fig. 7). Under the stable river discharge, the PC1 changed with the tidal

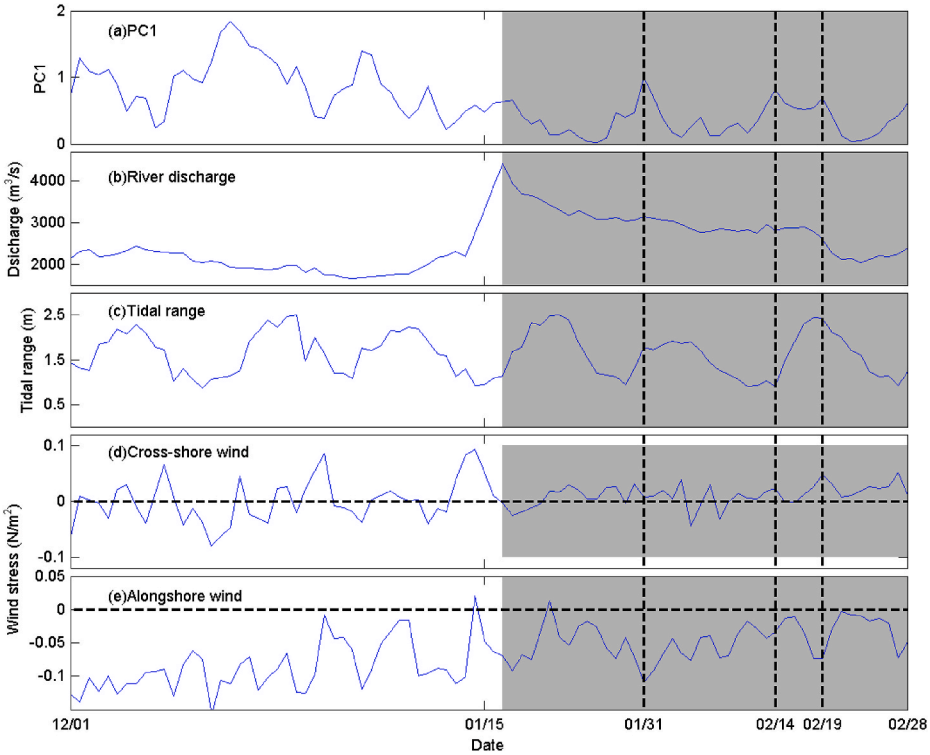

Fig. 10. Time series of the PC1(a), river discharge(b),tidal range(c),cross-shore wind stress(d), and alongshore wind stress (e) in 2014–2015. (The gray region represents the significant correlation between PC1 and river discharge in Fig. 5 of the wavelet-coherence spectra.)

Fig. 11. (a) Time series of the common power between the PC1 and alongshore wind from the cross-wavelet (blue line) and the river discharge (green line) from 2004 to 2015. (b) Time series of the common power (blue line) between the PC1 and alongshore wind from the cross-wavelet (blue line) and the alongshore wind (green line). (c) Time series of the common power between the PC1 and cross-shore wind from the cross-wavelet (blue line) and the river discharge (green line). (d) Time series of the common power between the PC1 and cross-shore wind from the cross-wavelet (blue line) and the cross-shore wind (green line).

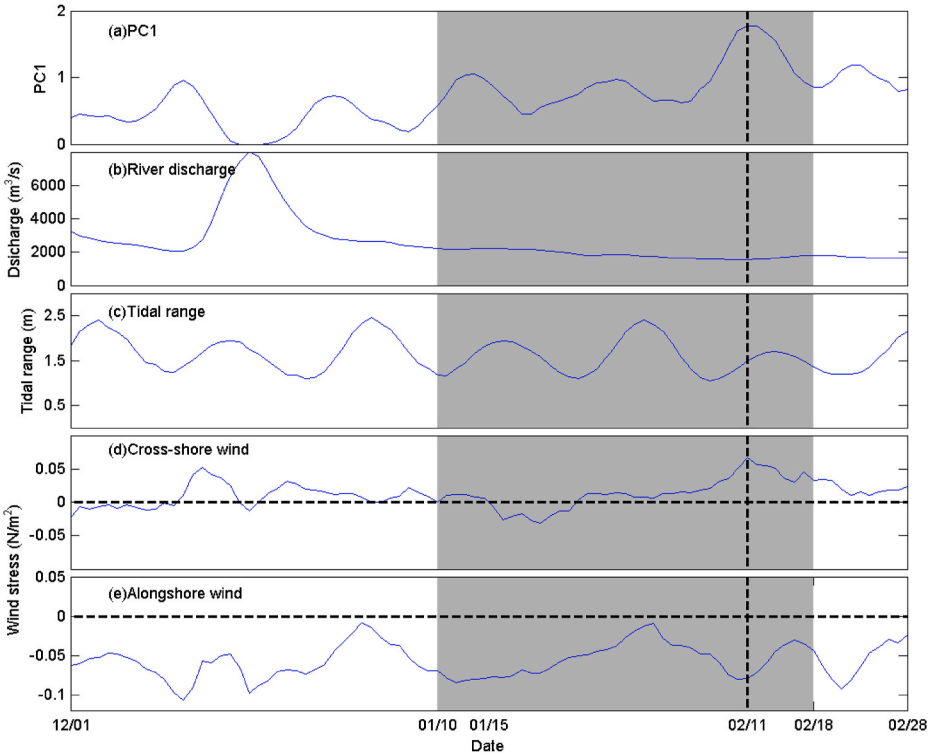

Fig. 12. Time series of the PC1(a), river discharge (b), tidal range (c), cross-shore wind stress (d), and alongshore wind stress (e) in 2013–2014. (The gray region represents the significant correlation between PC1 and cross-shore wind stress in Fig. 7 of the wavelet-coherence spectra.)

range. However, when the up-estuary wind and downwelling-favorable alongshore wind reached a maximum on February 11th, the PC1 attained a peak value, indicating that the winds played a key role in the salt intrusion. The up-estuary wind is generally regarded to decrease salt intrusion by reducing stratification and enhancing mixing. The downwelling-favorable alongshore wind has a positive effect on salt intrusion by landward Ekman transport and therefore elevated water level and salinity at the mouth.

The in-phase relationship between the PC1 and river discharge in 2014–2015 and that between the PC1 and up-estuary wind in 2013–2014 are both contrary to our general understanding. The in-phase relationship between the PC1 and river discharge was generated

by variations of tidal range and winds, as mentioned above. The in-phase relationship between the PC1 and up-estuary wind could be due to the increased surface landward flow by up-estuarywind, as our salinity data was obtained at the water surface.

Overall, from Tables 1–4, the sequence of importance in affecting the salt intrusion on the timescale of 12–17 days is the tidal range, cross-shore wind, alongshore wind, and river discharge. In Fig. 2a and b, when the fluctuation of river discharge was high, the salt intrusion decreased significantly. And there existed a high common power between the salt intrusion and river discharge in the timescale shorter than 12 days or longer than 17days in Fig. 5. Therefore, in timescales shorter than 12 days or longer than 17 days, the river discharge becomes more important.

4.4. Implication of this research to the regional water resource management

Gong and Shen (2011) and Lin et al. (2019) revealed that the salt intrusion is negatively correlated with tidal range in the Modaomen Estuary, that is, neap tide increases the salt intrusion, while spring tide weakens the salt intrusion. As shown in Figs. 10 and 12, the peaks of the salt intrusion usually occurred several days after the neap tides. Therefore, the salt intrusion lags the tidal range by approximately 1.8–6.2 days, which means that the severe salt intrusion lags the neap tide by 1.8–6.2 days, and the weak salt intrusion lags the spring tide by similar days. It suggests that the freshwater reservoirs need to have sufficient storage of 1.8–6.2 days after the spring tide to ensure safety of freshwater supply in the dry seasons.

Moreover, the water resources department generally released freshwater from the upstream reservoirs to restrain salt intrusion and safeguard the water supply downstream in the dry seasons. The salt intrusion lags the river discharge by approximately 1.2–9.2 days, indicating that the time and amount of freshwater released from the upstream reservoirs need to carefully take into account these time lags. In practice, the statistical probability distribution function (PDF) about the effect of upstream freshwater release on mitigating the salt intrusion can be obtained based on data analysis and numerical modeling.

Though the effects of winds on salt intrusion are significant, how to control these effects seems to be rather difficult. Thus, we do not discuss more the implication of the relationship between winds and salt intrusion here.

5. Summary

Based on the cross-wavelet and wavelet coherence analysis, this study discussed the response of salt intrusion to different forcing variables, including tidal range, river discharge, alongshore and cross-shore winds, in the timescale of 12–17 days (fortnightly) and other periodicities. We examined both the magnitude and time lag for the response. The main conclusions are drawn as follows:

1) The response time lags for the salt intrusion to the tidal range, river discharge, alongshore and cross-shore winds are 1.8–6.2, 1.2–9.2, 3.6–10.5, and 3.0–10.4 days, respectively.
2) For the time band of 12–17 days, when averaging the response magnitude in each winter over 2004–2016, the most important forcing variable in influencing the interannual variability of salt intrusion is the tidal range, followed by cross-shore wind, alongshore wind, and river discharge.

These time lags and the relative importance of different external forcings have implications for the freshwater resource management in the Modaomen Estuary.

3) The downwelling-favorable alongshore winds generally promote the salt intrusion by elevating the water level and salinity at the estuary and inducing landward flow inside the estuary. The down-estuary cross-shore winds have the same effect to enhance the salt intrusion by increasing the stratification in the estuary. The winds' effect is more important in the timescales less than 12 days or longer than 17 days.
4) The cross-wavelet and wavelet coherence are shown to be powerful tools for detecting the response of salt intrusion to changes in different external forcings. These tools are particularly useful when the processes are quite dynamic and the system stays in a transient state far from equilibrium. It also has the potential to analyze the processes in different timescale in a unified framework in the time-frequency space.

Through the wavelet analysis, we obtained the above preliminary results. Several questions are encountered in the analysis. For example, sometimes an increase in river discharge can cause an increase in salt intrusion, and an up-estuary wind can increase the salt intrusion and vice versa. These phenomena are contrary to the existing understanding. The physics behind such behaviors needs to be further explored in the future, and diagnostic study by numerical modeling would be adopted for future exploration.

Declaration of competing interest

The authors declare that they have no known competing financial interests or personal relationships that could have appeared to influence the work reported in this paper.

Acknowledgments

This research is funded by the National Natural Science Foundation of China [grant numbers: 51761135021, 41506102, 41606009].

References

Banas, N.S., Hickey, B.M., MacCready, P., Newton, J.A., 2004. Dynamics of Willapa Bay, Washington: a highly unsteady partially mixed estuary. J. Phys. Oceanogr. 34, 2413–2427.
Chen, S.-N., Sanford, L.P., 2009. Axial wind effects on salinity structure and longitudinal salt transport in idealized, partially mixed estuaries. J. Phys. Oceanogr. 39, 1905–1920.
Chen, S.-N., 2015. Asymmetric estuarine response to changes in river forcing: a consequence of nonlinear salt flux. J. Phys. Oceanogr. 45, 2836–2847.
Farge, M., 1992. Wavelet transforms and their applications to turbulence. Annu. Rev. Fluid Mech. 24 (1), 395–458.
Fong, D., Geyer, W., 2001. Response of a river plume during an upwelling favorable wind event. J. Geophys. Res. 106 (C1), 1067–1084.
Forbes, D.J., Xie, Z., 2018. Identifying process scales in the Indian River Lagoon, Florida using wavelet transform analysis of dissolved oxygen. Ecol. Complex. 36, 149–167.
Gong, W., Shen, J., 2011. Response of saltwater intrusion to changing river flow and tidal amplitude during winter season in the Modaomen Estuary, Pearl River Delta area, China. Continent. Shelf Res. 31, 769–788.
Grinsted, A., Moore, J.C., Jevrejeca, S., 2004. Application of the cross wavelet transform and wavelet coherence to geophysical time series. Nonlinear Process Geophys. 11 (5/6), 561–566.
Kranenburg, C., 1986. A timescale for long-term salt intrusion in well-mixed estuaries. J. Phys. Oceanogr. 16, 1329–1331.
Lerczak, J.A., Geyer, W.R., Ralston, D.K., 2009. The temporal response of the length of a partially stratified estuary to changes in river flow and tidal amplitude. J. Phys. Oceanogr. 39, 915–933.
Li, Y., Li, M., 2011. Effects of winds on stratification and circulation in a partially mixed estuary. J. Geophys. Res. 116, C12012. https://doi.org/10.1029/2010JC006893.
Li, Y., Li, M., 2012. Wind-driven lateral circulation in a stratified estuary and its effects on the along-channel flow. J. Geophys. Res. 117, C09005. https://doi.org/10.1029/2011JC007829.
Lin, Z., Zhang, H., Lin, H., Gong, W., 2019. Intraseasonal and interannual variabilities of saltwater intrusion during dry seasons and the associated driving forcings in a partially mixed estuary. Continent. Shelf Res. 174, 95–107.
Liu, B., Yan, S., Chen, X., Lian, Y., Xin, Y., 2014. Wavelet analysis of the dynamic characteristic of saltwater intrusion- A case study in the Pearl River Estuary of China. Ocean Coast Manag. 95, 81–92.
Lonnie, H., Huang, J.P., 1996. Bivariate wavelet analysis of Asia monsoon and ENSO. Adv. Atmos. Sci. 13 (3), 299–312.
MacCready, P., 1999. Estuarine adjustment to changes in river flow and tidal mixing. J. Phys. Oceanogr. 29, 708–726.

MacCready, P., 2007. Estuarine adjustment. J. Phys. Oceanogr. 37, 2133–2145.
MacCready, P., Geyer, R.W., 2010. Advances in estuarine physics. Ann. Rev. Mar. Sci 2, 35–58.
North, E.W., Chao, S.Y., Sanford, L.P., Hood, R.R., 2004. The influence of wind and river pulses on an estuarine turbidity maximum: numerical studies and field observations in the Chesapeake Bay. Estuaries 27 (1), 132–146.
Scully, M.E., Friedrichs, C., Brubaker, J., 2005. Control of estuarine stratification and mixing by wind-induced straining of the estuarine density field. Estuaries 28 (3), 321–326.
Torrence, C., Compo, G.P., 1998. A practical guide to wavelet analysis. Bull. Am. Meteorol. Soc. 79 (1), 61–78.
Yuan, Y., Yang, C., Tseng, Y., Zhu, X., Wang, H., Chen, H., 2017. Analysis of longer period variation of the Kuroshio Current intrusion into the Luzon Strait using rectified wavelet power spectra. Prog. Oceanogr. 156, 61–77.